

Peer review status:

This is an under-peer-review preprint submitted to EarthArXiv.

1 Large earthquakes are more predictable than smaller ones

2 Patricio Venegas-Aravena^{1,*} and Davide Zaccagnino^{2,3,**}

3

- 4 1. Independent Researcher, 4030000, Concepción, Chile
- 5 2. Institute of Risk Analysis, Prediction & Management (Risks-X), Southern University of
6 Science and Technology (SUSTech), 1088 Xueyuan Blvd, Nanshan, 518055, Shenzhen, China.
- 7 3. National Institute of Geophysics and Volcanology (INGV), Via di Vigna Murata, 605, 00143,
8 Rome, Italy.

9

10 * plvenegas@uc.cl

11 ** zaccagnino@sustech.edu.cn

12

13 Orcid:

14 P.V.-A.: <https://orcid.org/0000-0003-3777-0941>

15 D.Z.: <https://orcid.org/0000-0001-6884-8452>

16

17 Author contributions statement

18 P.V.-A.: Conceptualization, Formal analysis, Investigation, Methodology, Project Administration,
19 Software, Resources, Supervision, Validation, Visualization, Writing – original draft and review &
20 editing; D.Z.: Conceptualization, Data Curation, Formal analysis, Funding Acquisition, Investigation,
21 Methodology, Software, Validation, Visualization, Writing – original draft and review & editing.

22

23 Abstract

24 Large earthquakes have been viewed as highly chaotic events regardless of their magnitude,
25 making their prediction intrinsically challenging. Here, we develop a mathematical tool to
26 incorporate multiscale physics, capable of describing both deterministic and chaotic systems, to
27 model earthquake rupture. Our findings suggest that the chaotic behavior of seismic dynamics,
28 that is, its sensitivity to initial and boundary conditions, is inversely related to its magnitude. To
29 validate this hypothesis, we performed numerical simulations with heterogeneous fault conditions.
30 Our results indicate that large earthquakes, usually occurring in regions with higher residual energy
31 and lower b-value (i.e., the exponent of the Gutenberg-Richter law), are less susceptible to be
32 affected by perturbations. This suggests that a higher variability in earthquake magnitudes (larger
33 b-values) may be indicative of structural complexity of the fault network and heterogeneous stress
34 conditions. We compare our theoretical predictions with the statistical properties of seismicity in
35 Southern California; specifically, we show that our model agrees with the observed relationship
36 between the b-value and the fractal dimension of hypocenters. The similarities observed between
37 simulated and natural earthquakes support the hypothesis that large events may be less chaotic
38 than smaller ones; hence, more predictable.

39

40 **Keywords:** Earthquake predictability; Seismic rupture; Chaos theory; Residual energy; b-value; HE-
41 B method.

42

43 1. Introduction

44 Earthquakes are a persistent threat to human society, capable of causing widespread devastation
45 (e.g., Kahandawa et al., 2018). The rapid release of accumulated tectonic stress can result in
46 catastrophic natural disasters with severe human and economic consequences (Knopoff, 1958;
47 Vassiliou and Kanamori, 1982; Gudmundsson, 2014; Aksoy et al., 2024; Silverio-Murillo et al.,

48 2024). To efficiently face seismic risk, a deeper understanding of seismicity is needed. Particularly,
49 a fundamental aspect of earthquake studies is the examination of rupture processes along
50 geological faults (e.g., Christensen and Beck, 1994; Kintner et al., 2018; Otarola et al., 2021;
51 Martínez-Lopez, 2023; Wang et al., 2023), as these can induce notable changes in the soil's
52 physical characteristics, such as variations in ground velocity, acceleration and frequency (Colavitti
53 et al., 2022; Li et al., 2022; Venegas-Aravena, 2024a). Evidence from various studies points to the
54 possibility that seismic rupture processes may exhibit the hallmarks of chaotic systems, suggesting
55 a complex and unpredictable nature of these events. Some perspectives on earthquake generation
56 are rooted in simplified spring-block models which exhibit these chaotic dynamics (e.g., Huang and
57 Turcotte, 1990; Gualandi et al., 2023). This is reflected in computational simulations where small
58 variations in the initial conditions generate completely different rupturing scenarios (e.g., Erickson
59 et al., 2011). That is, causing no correlation between a priori and a posteriori parameter (Venegas-
60 Aravena et al., 2024). Despite this complexity, a consistent finding from these simulations is the
61 emergence of a single dominant parameter: residual energy. The importance of the
62 accumulated/residual strain is also coherent with recent results in the modeling of paleoseismic
63 recordings (Salditch et al., 2020). This parameter, which defines zones where ruptures are prone to
64 occur (Noda et al., 2022), appears to exert a controlling influence on both the spatial extent and
65 temporal evolution of ruptures (Venegas-Aravena, 2023; Venegas-Aravena et al., 2024). Its value is
66 dependent on both the available energy, which is determined by the initial stresses, and the
67 fracture energy, which is associated with the energy required to continue propagating the rupture
68 (Noda et al., 2022). Therefore, when the rupture front approaches a zone with negative (positive)
69 stress release rate, more (less) energy is consumed in generating the rupture, causing the rupture
70 to arrest (continue propagating). Other formalisms associated with friction have also found that
71 rupture arrest can be related to stresses and fracture energy (Barras et al., 2023).

72
73 Residual energy has been linked to a parameter called thermodynamic fractal dimension D
74 (Venegas-Aravena and Cordaro, 2023a). This quantity is useful for characterizing fault distribution
75 (Zou and Fialko, 2024) and the spatial distribution of global seismicity (Perinelli et al., 2024). For
76 instance, it has been observed that the fractal dimension decreases prior to a major earthquake,
77 suggesting a transition from a more diffuse, three-dimensional seismicity distribution to a more
78 localized, planar distribution along the fault (Murase, 2004; Wyss et al., 2004; Iaccarino and Picozzi,
79 2023). Other studies have interpreted this decrease in D as an indicator of an impending larger
80 rupture due to the increase of shear stresses (e.g., Ito and Kaneko, 2023; Venegas-Aravena and
81 Cordaro, 2023a). Furthermore, it has been linked to the b-value, a parameter describing
82 earthquake frequency (Venegas-Aravena and Cordaro, 2023b). Given the proportional relationship
83 between D and the b-value, a decrease in D is also associated with a decrease in the b-value prior
84 to large earthquakes. Given the link between the parameter D and properties associated with
85 chaotic systems, as suggested by lower D values in less chaotic systems (Venegas-Aravena and
86 Cordaro 2024), the b-value is anticipated to provide insights into the chaotic states of faults. To
87 explore this connection, Section 2 delves into the fundamental principles of multiscale
88 thermodynamics applied to faults. Section 3 presents various simulations of heterogeneous
89 ruptures, facilitating the interpretation of parameters such as D and the b-value within the
90 framework of multiscale thermodynamics and chaotic systems. In Section 4, we apply these
91 concepts to a real fault system, specifically in Southern California, to support our theoretical and
92 numerical results. A discussion and conclusion are presented in Sections 5 and 6 respectively.

93
94

95 2. Theoretical background: multiscale thermodynamics

96 As earthquakes are essentially multi-scale events that may exhibit chaotic behavior, a physical
97 framework is required to fully understand their dynamics. In this regard, Venegas-Aravena and
98 Cordaro (2024), have developed a quantitative relationship linking the sum of the Lyapunov
99 exponents Λ , to the thermodynamic fractal dimension D , expressed as:

$$100 \Lambda \sim -e^{(D_E - D - 1)/k_V} \quad (1)$$

101 The Euclidean dimension is denoted by D_E , while k_V is a constant associated with the system's
102 scale. D is a parameter that characterizes the distribution of systems exhibiting power-law behavior.

103
104 While Lyapunov exponents are related to the eigenvalues of the Jacobian matrix, describing the
105 local stability of a system (e.g., Wu and Baleanu, 2015), Equation 1 is inspired by the work of
106 Hoover and Posch (1994), wherein the summation of exponent pairs in non-equilibrium systems is
107 employed to quantify irreversibility and the loss of phase-space dimensionality associated with
108 dissipative processes such as frictional heat generation and the occurrence of earthquakes,
109 thereby providing a complementary perspective to purely local analysis.

110
111 It is also paramount to comprehend the physical significance of Equation 1. The parameter Λ ,
112 representing the sum of the Lyapunov exponents, describes the global tendency of the system
113 towards contraction or dilation of volume in phase space, reflecting overall dissipation or
114 instability (e.g., Eden et al. (1991)). In contrast, the internal dynamics of a dissipative system,
115 including the thermodynamic forces and fluxes that drive entropy production, are described at the
116 microscopic level by the Onsager coefficients (Onsager, 1931a; 1931b). The introduction of the
117 parameter D within multiscale thermodynamics framework implies that dissipative processes are
118 described by a generalization of the Onsager coefficients, which operate across a range of scales. In
119 this context, D serves as a conceptual bridge, enabling the linkage of dynamics occurring at smaller
120 scales, where the common thermodynamic forces and fluxes manifest, with the global evolution of
121 the system observed in the macroscopic phase space. In this manner, D quantifies the organization
122 of dissipation and fluctuations across these multiple scales, thereby influencing the global stability
123 of the system as characterized by Λ .

124
125 This Equation can be observed in Figure 1a for $k_V = 1$, where low (large) values of Λ are associated
126 with low (large) values of D . A higher value of Λ indicates that the system is more susceptible to
127 the influence of small changes in initial conditions (Ruelle, 1983; Tabor, 1989), whereas a more
128 negative value of Λ suggests that the system is less sensitive to these initial conditions, which
129 could be considered as being more regular. The sign of Λ provides an indication of whether a
130 system is non-reversible/dissipative (negative sum) or conservative (e.g., Hoover and Posch, 1994).
131 Given that the brittle crust is a system characterized by the dissipation of stored energy, the sum of
132 Λ is a more relevant metric than the largest Lyapunov exponent, often used to determine the
133 chaotic nature of a system. Consequently, lower values of D correspond to less chaotic systems,
134 i.e., less sensitive to initial conditions. In the case of earthquakes, D can be related to the
135 magnitude of seismic events through the equation (Venegas-Aravena and Cordaro 2023a):

$$136 M_W \sim \log_{10}(e^{-\alpha(D)}) \quad (2)$$

137 Where $\alpha(D) = pD/k_V$ and $p = 3/(5 - D)$. From Equation 1, D can be written in terms of the
138 sum of the Lyapunov exponent as $D = (D_E - 1) - k_V \ln \Lambda$. By substituting this Equation into
139 Equation 2, we can establish a direct relationship between the magnitude and chaotic systems as:

$$140 M_W = M_W(\Lambda) \quad (3)$$

141 This relationship is graphically depicted in the color-coded maps presented in Figures 1a, 1b, and
 142 1c. In these maps, red tones correspond to earthquakes of greater magnitude, while blue tones
 143 represent smaller earthquakes. It should be noted that the apparent deviation of Figure 1,
 144 particularly Figure 1a where Equation 1 is plotted, from typical exponential functions is
 145 attributable to the restricted range employed for D (between 2 and 3) and the specific selection of
 146 k_V . A broader range for D and/or alternative values of k_V may result in graphs exhibiting a more
 147 visually exponential form.

148 In Figure 1a, large earthquakes are correlated with lower values of both D and Λ . This finding
 149 implies that larger seismic events exhibit a reduced sensitivity to initial conditions. In contrast,
 150 smaller earthquakes (represented by blue hues in Figure 1a) are associated with a higher degree of
 151 chaos, suggesting that these events originate in a more chaotic environment where even small
 152 perturbations can lead to seismic activity of varying scales, from small to intermediate. This
 153 phenomenon is coherent with several observations suggesting the strong sensitivity of small
 154 seismicity to stress perturbations, e.g., tides and hydrological modulations (Rubinstein et al., 2008;
 155 Petrelis et al., 2021), which are not reported for major events (Vidale et al., 1998).

156
 157 Figure 1a also illustrates that the values of Λ are negative, which might suggest that the system is
 158 not chaotic as described. However, it is important to differentiate between individual Lyapunov
 159 exponents and their summation. While a negative sum of all Lyapunov exponents indicates a
 160 contraction, due to energy dissipation, of the global phase-space volume, the presence of even a
 161 single positive Lyapunov exponent is the defining characteristic of chaos. This positive exponent
 162 signifies the exponential divergence of initially infinitesimally close trajectories along a specific
 163 direction in phase space, leading to the unpredictability and sensitive dependence on initial
 164 conditions characteristic of chaotic systems. Therefore, a system can exhibit a net dissipative
 165 behavior (negative sum) and still be fundamentally chaotic due to the local instability introduced
 166 by at least one positive Lyapunov exponent, which drives the complex and seemingly random
 167 evolution of its dynamics.

168
 169 To delve deeper into this phenomenon, it is imperative to examine the energy conditions within
 170 the fault, specifically the concept of residual energy, E^{res} (Noda et al., 2021). This energy
 171 parameter serves as a criterion for the initiation of ruptures, indicating that a positive E^{res} value
 172 signifies a greater propensity for a fault to generate ruptures, while negative values diminish this
 173 likelihood. Mathematically, this energy can be expressed as:

$$174 \quad E^{res} = \Delta W_0 - G_C \quad (4)$$

175 Where ΔW_0 represents the available energy, which can be correlated with the elastic energy stored
 176 within the system, and G_C denotes the fracture energy, characterizing the resistance to rupture
 177 propagation. It is also important to note that residual energy can be regarded as equivalent to
 178 radiated energy, which refers to the energy radiated to the medium which is transported by
 179 seismic waves (e.g., Rivera and Kanamori, 2005; Venegas-Aravena, 2024a). Despite this
 180 equivalence, the concept of residual energy as defined by Noda et al. (2021) more closely aligns
 181 with the processes occurring within the fault and its heterogeneities. Therefore, given the
 182 emphasis in this work on the generation of ruptures within faults, rather than the propagation of
 183 seismic energy through a medium, the concept of residual energy has been adopted. Equation 4
 184 can be expressed in terms of D as follows (Venegas-Aravena and Cordaro, 2023a):

$$185 \quad E^{res} \sim e^{-D/2k_V} - d_0^D \quad (5)$$

186 Where d_0 is constant.

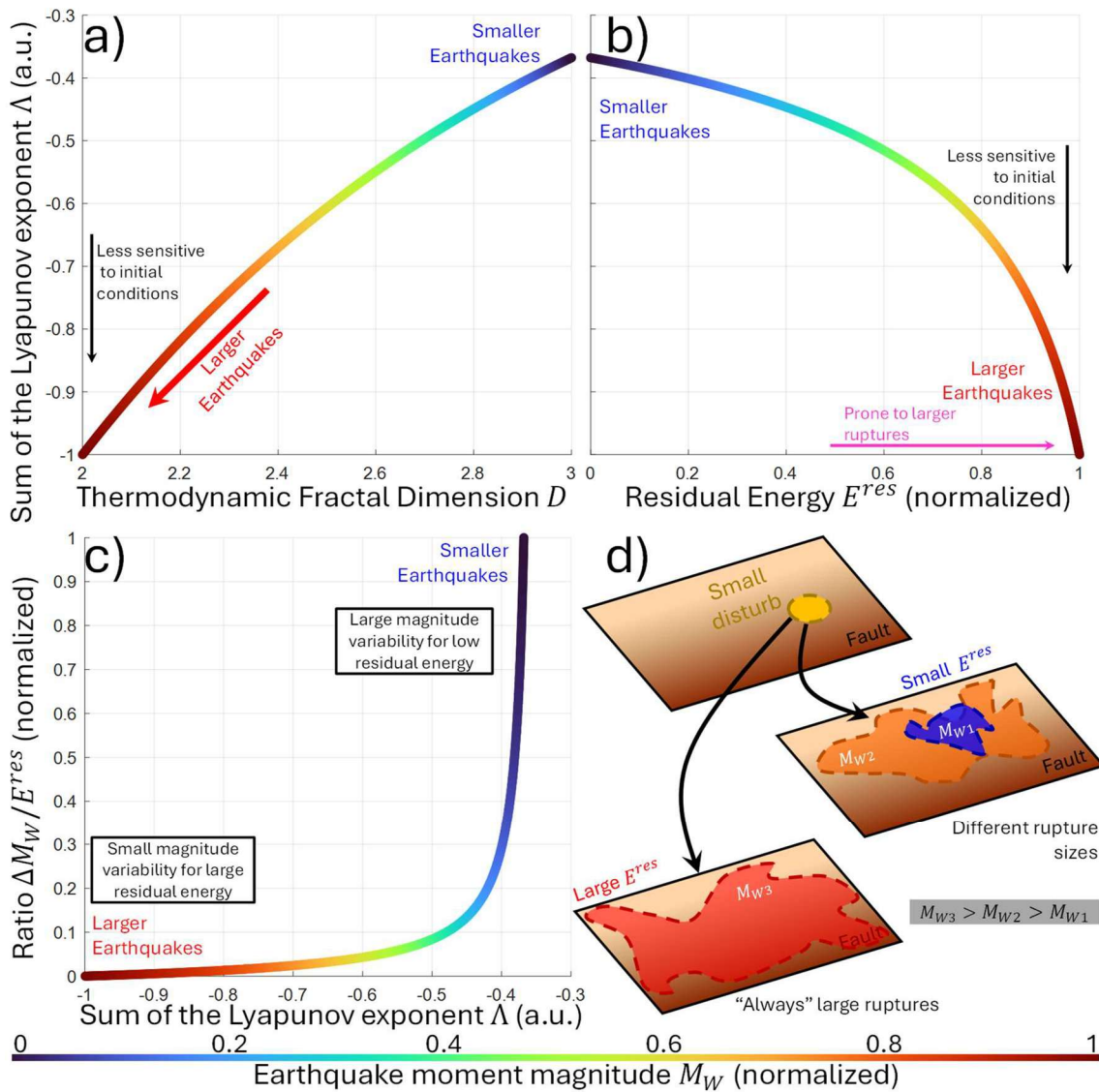
187 At this juncture, it is pertinent to elucidate the relationship among the fractal dimension, the
188 Euclidean dimension, and earthquake magnitude through the residual energy as described by
189 Equation 5. Within the framework of this study, D_E represents the dimension of the Euclidean
190 space in which the spatial distribution of earthquake epicenters, and their ruptures, is embedded
191 and subsequently analyzed to derive an empirical fractal dimension. Specifically, D_E defines a
192 volume and is therefore equal to 3. In the context of multiscale thermodynamics, the fractal
193 dimension D serves as a global parameter of the fault, quantifying its geometric irregularities and,
194 consequently, its fracture energy (e.g., Xie, 1994). The connection to magnitude lies in the fact that
195 lower values of D imply a reduced fracture energy, leading to a larger area of positive residual
196 energy and, as a result, a higher probability of the occurrence of earthquakes with greater
197 magnitude M_W (Venegas-Aravena and Cordaro, 2023a; Venegas-Aravena, 2024b). Consequently,
198 the fractal dimension of the spatial distribution of earthquakes, ascertained within a Euclidean
199 space, is indirectly related to magnitude through its association with the global parameter D of the
200 fault.

201

202 Figure 1b illustrates the relationship between E^{res} , Λ , and earthquake magnitude (color-coded
203 map). Higher E^{res} values correlate with lower Λ values, suggesting that regions more prone to
204 rupture are also less sensitive to initial conditions. Given that these regions are associated with
205 large earthquakes (red colors), it is proposed that areas with high residual energy have higher
206 chances to host a major event as a response to stress perturbations.

207

208



209

210

211 **Figure 1: a) Equation 1 reveals a relationship between the sum of Lyapunov exponents Λ and the**
 212 **thermodynamic fractal dimension D . Systems with low sensitivity to initial conditions (highly**
 213 **negative Λ values) correspond to low D values. Colors indicate event magnitudes as calculated**
 214 **by Equation 2. Large events (red hues) are associated with low D and low Λ . b) Equation 5**
 215 **relates Λ to residual energy (E^{res}). Higher E^{res} values correlate with a higher probability of large**
 216 **earthquakes, which in turn are linked to lower chaos and larger events. c) The plot of magnitude**
 217 **changes for a given E^{res} versus Λ shows that small (large) earthquakes exhibit greater (lesser)**
 218 **magnitude variability for low (high) E^{res} , as indicated by blue (red) hues. d) A schematic**
 219 **illustrates how perturbations can trigger small-to-medium or large earthquakes depending on**
 220 **E^{res} .**

220

221

222 To visualize this, Figure 1c shows the variation in magnitude ΔM_W relative to residual energy. This
 223 figure illustrates the change in magnitude resulting from the addition of a small quantity of
 224 residual energy to a fault, in comparison to the same fault without this increase in energy. The
 225 findings indicate that introducing a small amount of residual energy can significantly elevate the
 226 expected magnitude (relative to the expected magnitude of the same fault without this additional
 227 energy) when the initial residual energy is low. Conversely, if the initial residual energy is already

228 high, the addition of the same small quantity of energy produces a comparatively minor change in
229 the expected magnitude (relative to the fault without this additional energy), suggesting a
230 saturation effect on the magnitude. That is, the variation in M_W is small (large) when E^{res} is high
231 (low). This supports the notion that there is a more restricted range of possible earthquakes when
232 the residual energy in the fault is higher. Figure 1d schematically depicts this concept: a fault with a
233 small E^{res} can generate earthquakes of magnitudes M_{W1} (blue area) and M_{W2} (orange area),
234 whereas in the case of a large E^{res} , only earthquakes of magnitude M_{W3} (red area) can be
235 generated, which is larger than both M_{W1} and M_{W2} .

236

237

238 3. Simulations

239 3.1 Heterogeneous Energy-Based method

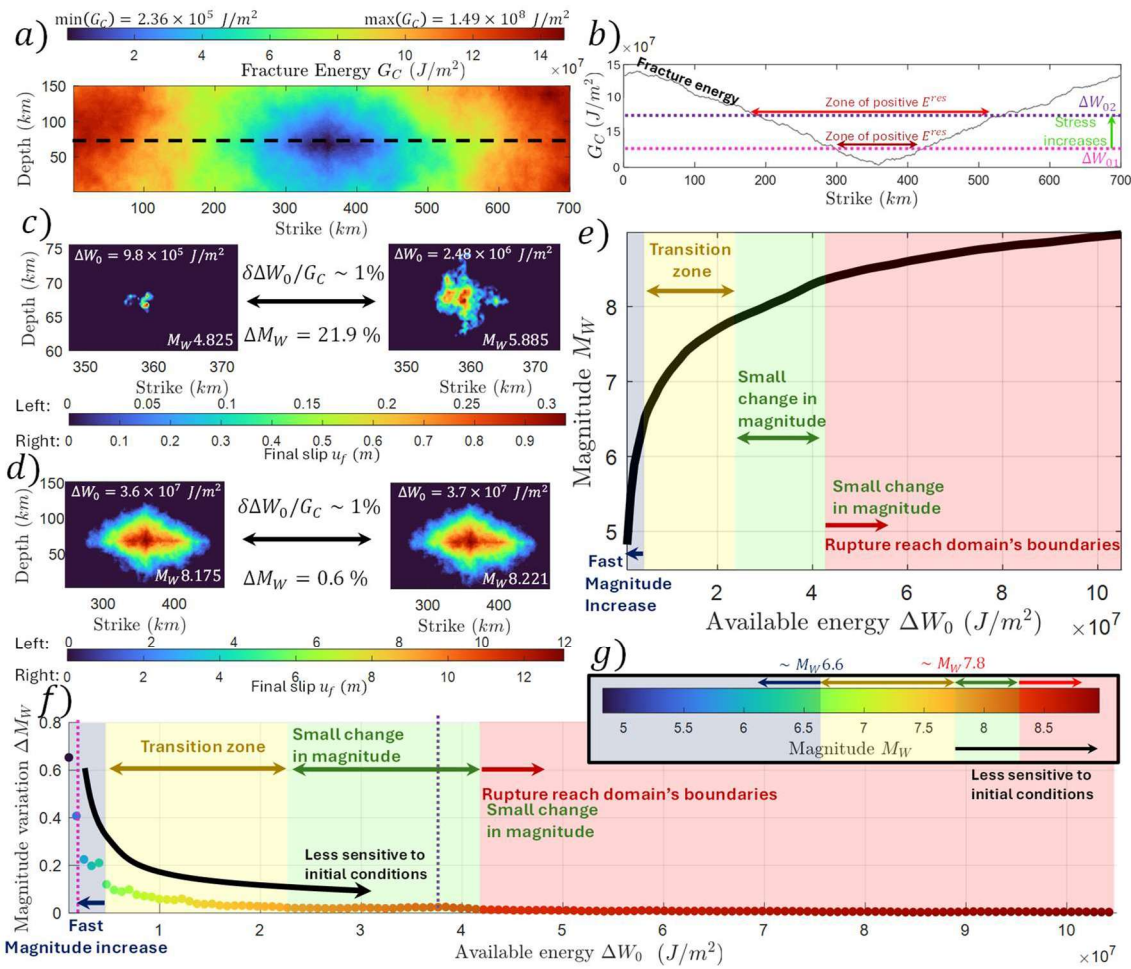
240 The heterogeneous energy-based method (HE-Bm) posits that seismic rupture propagation is
241 governed by the heterogeneous distribution of residual energy (Venegas-Aravena, 2023). This
242 model suggests that rupture velocity and slip magnitude at each point on the fault are directly
243 correlated with the residual energy. Consequently, regions with high residual energy are more
244 prone to experiencing large slip u_f and high rupture velocities v_r , which can potentially lead to
245 larger magnitude earthquakes. Thus, the relation between slip and residual energy is $u_f \propto E^{res}$.

246 According to the framework of HE-Bm, E^{res} can be linked to the distribution of interseismic
247 coupling on a fault through the concept of available energy, while fault geometry is related to
248 residual energy via fracture energy (Venegas-Aravena and Cordaro, 2023a). The two-dimensional
249 fractal dimension D of natural fractures have been determined to be 2.3 (Huang et al., 1992).
250 Consequently, due to the proportional relationship between the fracture energy G_C and the
251 geometric variations of the fracture (e.g. Xie, 1993), it is expected that G_C will also possess a fractal
252 dimension of 2.3.

253

254 3.2 Ruptures in a single distribution of G_C

255 Figure 2a presents an exemplar G_C distribution exhibiting a fractal dimension of 2.3. The strike and
256 depth are 700 km and 150 km respectively. The spacing is 349.5 m for the strike and 371.6 m for
257 the depth. This distribution was constructed through the interpolation of random values,
258 employing the methodology outlined by Chen and Yang (2016). Given the established inverse
259 correlation between elevated G_C values and rupture size (Renou et al., 2022), attributed to the
260 self-arresting nature of ruptures induced by energy depletion, the central region (depicted in blue
261 in Figure 1a) was intentionally constrained to be three orders of magnitude less than the
262 peripheral regions (rendered in red). Note that the arrest of ruptures due to geometric changes
263 (fracture energy) has also been observed in real faults (e.g., Padilla et al., 2024). Consequently,
264 ruptures are invariably localized within the lower G_C value domains (represented by the blue hues
265 in Figure 1a). As coupling seems to be related to stress (Wallace et al., 2012), this implies that for a
266 given level of stress on a fault, it is the fault roughness that primarily determines residual energy.
267 Smoother faults exhibit lower fracture energy, resulting in reduced resistance to rupture initiation
268 and, consequently, larger rupture events. Conversely, rougher faults present higher fracture energy,
269 limiting residual energy and thus constraining rupture size.

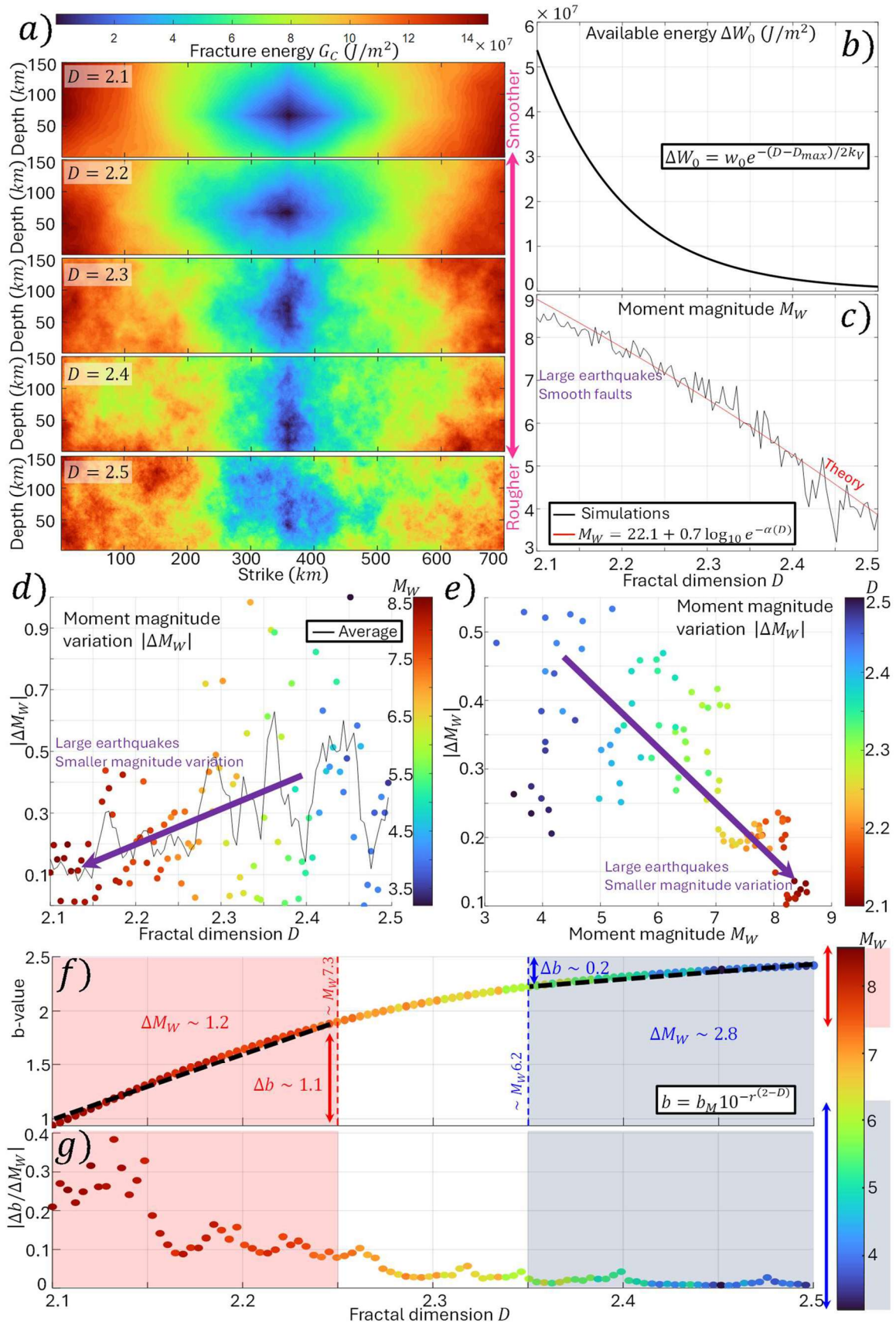


270
 271 **Figure 2: a) Example of fracture energy distribution with $D=2.3$, where the central region has low**
 272 **values, and the edges have high values. b) Fracture energy profile corresponding to the**
 273 **segmented black line in a). Magenta and purple segmented lines indicate two levels of available**
 274 **energy ΔW_0 . Dark red and red double arrows indicate the size of positive E^{res} , potentially**
 275 **corresponding to rupture size. c) and d) shows the final slip distributions for conditions of low**
 276 **and high available energy, respectively. c) reveals larger changes in magnitude than those shown**
 277 **in d). e) The relationship between moment magnitude and ΔW_0 is shown. The gray region**
 278 **highlights a rapid increase in magnitude with increasing ΔW_0 , while the yellow and green zones**
 279 **show a decreasing rate of increase. The red zone indicates ruptures that reach the fault edges. f)**
 280 **The variation of magnitude with available energy for different values of the parameter ΔW_0 is**
 281 **shown. Lower values of ΔW_0 result in larger changes in magnitude. g) The color map used in f),**
 282 **which indicates the sensitivity of earthquakes to initial conditions: blue for smaller earthquakes**
 283 **($M_W \sim 6.6$), yellow for a transition region (M_W between 6.6 and 7.8), and red for larger**
 284 **earthquakes ($M_W > 7.8$) that are less sensitive.**

285
 286

287 Equivalently, for a given fracture energy distribution, the residual one will be determined by the
 288 amount of available energy. This example is shown in Figure 2b. The black curve corresponds to a
 289 trace indicated by the black segmented line in Figure 2a. The minimum value is $G_C = 2.36 \times$
 290 10^5 J/m^2 , which is found approximately at the midpoint of the fault (strike of 350 km). These
 291 values of G_C tend to increase towards the strike equal to zero km and equal to 700 km. The
 292 segmented magenta and purple lines represent two uniform distributions of available energy,
 293 ΔW_{01} and ΔW_{02} , respectively. In this case, ΔW_{02} is greater than ΔW_{01} , indicating that the first case

294 has a smaller amount of accumulated stress on the fault than the second case. The dark red
295 double arrow would indicate the zone with positive residual energy given the level of ΔW_{01} , which
296 is equivalent to a potential rupture zone. The red double arrow indicates the zone of positive
297 residual energy given a higher accumulated stress (given by ΔW_{02}). This zone is wider than the
298 region marked by the dark red arrow, highlighting the presence of larger ruptures promoted by
299 high stress values throughout the crustal volume. The increase of available energy also translates
300 into changes in earthquake magnitudes. For instance, Figure 2c illustrates two ruptures initiated
301 with similar available energy ($10^6 J/m^2$), representing a one percent variation relative to the
302 maximum fracture energy. This excess in available energy defines the positive residual energy area
303 (rupture area A), which can be related to the seismic moment M_0 through the empirical
304 relationship $M_0 = \mu C_2 A^{3/2}$, where μ is the shear modulus with a value of $40 GPa$ and C_2 is a
305 dimensionless constant equal to 3.8×10^{-5} (Leonard, 2010). The small variation available energy
306 results in a $\sim 22\%$ increase in earthquake magnitude (from M_W 4.8 to M_W 5.9). Conversely, when
307 the available energy is higher ($\sim 3.6 \times 10^7 J/m^2$), a similar 1% increase produces earthquakes
308 with nearly identical magnitudes (M_W 8.2 representing a variation smaller than 1%, as shown in
309 Figure 2d), suggesting that faults with higher residual energy yield similar magnitude earthquakes.
310 The dependence of magnitude on available energy is depicted in Figure 2e. This figure shows 140
311 simulations with different values of ΔW_0 . A significant increase in magnitude is observed for low
312 available energy values, indicated by the blue region. In this region, a small increase in ΔW_0 (less
313 than $10 MJ/m^2$) can elevate an earthquake from magnitudes less than 5 to approximately M_W 6.6.
314 The yellow and green regions show a less pronounced increase in magnitude compared to the blue
315 region. The red range represents events where the ruptures approach the fault boundaries. The
316 magnitude change in this region appears unaffected by fault boundary influences. Figure 2f
317 quantifies these variations, revealing that the blue region experiences ΔM_W values close to 0.7,
318 while the green and red regions show negligible changes. The color map in Figure 2g corroborates
319 these findings, with earthquakes smaller than M_W 6.6 predominantly falling within the blue region
320 and larger earthquakes (M_W larger than M_W 7.8) exhibiting minimal sensitivity to variations in ΔM_W .
321
322
323
324
325
326
327
328
329
330
331
332
333
334
335
336
337
338
339
340



341
342
343
344
345
346
347
348
349
350
351
352
353
354
355
356
357
358
359
360
361
362
363
364
365
366
367
368
369
370
371
372
373
374
375
376
377
378
379
380
381
382

383 **Figure 3:** a) Fracture energy of a fault with different fractal dimension (D) values. The
384 distribution becomes rougher as D increases. b) There is an exponential relationship between
385 available energy and D . As D decreases, the available energy increases exponentially. c) The
386 relationship between moment magnitude and D is shown. The simulated data is represented by
387 the black curve, and the theoretical prediction by Venegas-Aravena and Cordaro (2023a) is

388 shown in red. d) and e) show the relationship between fractal dimension, moment magnitude,
 389 and magnitude variation. The purple arrow indicates that in both figures, low values of D are
 390 associated with high-magnitude earthquakes and small magnitude variations. That is, a small
 391 change in D , when ΔW_0 values are high, almost always generates similar large earthquakes.
 392 When ΔW_0 values are low, there is a greater variation in magnitude. f) Relationship between b-
 393 value and D . There is a greater decrease in the b-value when there are larger earthquakes. g)
 394 Variation of the b-value with changes in M_W . This variation is greater when D is lower.

395
 396

397 3.3 Ruptures with different G_C

398 While natural faults can be characterized by a fractal dimension of approximately 2.2 (e.g. Kagan,
 399 1991), variations in this value are possible. To investigate the impact of fractal dimensions on
 400 fracture energy, 100 simulations were conducted with fractal dimensions ranging from 2.1 to 2.5.
 401 Figure 3a illustrates examples of fault geometries with fractal dimensions of 2.1, 2.2, 2.3, 2.4, and
 402 2.5, respectively, where maximum and minimum G_C values are consistent with Figure 2a. In these
 403 simulations, lower G_C values are maintained at the fault center and higher values at the edges. As
 404 shown in Figure 3a, the distribution of G_C becomes smoother as the fractal dimension approaches
 405 2.1.

406 As suggested by Venegas-Aravena and Cordaro (2023a), ΔW_0 is inversely related to D , with the
 407 specific relationship being $\Delta W_0 \sim e^{-D/2k_V}$. Therefore, any change in G_C must be accompanied by
 408 a corresponding change in ΔW_0 . Figure 3b visualizes this relationship using parameter values of
 409 $w_0 = 9.84 \times 10^5 J/m^2$, $D_{max} = 2.5$ and $k_V = 0.05$. These values yield a range of ΔW_0 consistent
 410 with the previous section, ensuring that ΔW_0 is sufficiently large to allow for rupture initiation but
 411 not so large as to be influenced by domain boundaries. The figure clearly demonstrates that lower
 412 values of D are associated with higher values of ΔW_0 , indicating smoother spatial distributions of
 413 G_C . The magnitude of these ruptures also varies as a function of D . In Figure 3c, the red curve
 414 represents the theoretical relationship proposed by Venegas-Aravena and Cordaro (2023a), given
 415 by Equation 2. The observed magnitudes, depicted by the black curve, align well with the
 416 theoretical values. However, a higher variability in magnitude $|\Delta M_W|$ is observed for larger values
 417 of D (greater than 2.4), while lower values of D (less than 2.3) exhibit lower variability. This
 418 variation is visualized in Figure 3d, where the color map indicates magnitude. The black curve in
 419 Figure 3d represents a 5-point moving average of $|\Delta M_W|$, with the purple arrow highlighting the
 420 trend towards lower magnitude variability for smaller values of D . Figure 3e explicitly shows the
 421 relationship between M_W and its average variability (in this case a 10-point moving average), with
 422 the color map indicating D values. As the purple arrow suggests, there is an inverse correlation
 423 between M_W and its average variability, where earthquakes with magnitudes less than $M_W \sim 5$ can
 424 exhibit magnitude differences greater than $0.5M_W$. In contrast, for earthquakes with magnitudes
 425 greater than $M_W \sim 8$, this variability decreases to approximately $0.1M_W$.

426

427 3.4 Chaos and b-value

428 Both laboratory and field studies have shown a negative correlation between the b-value, which
 429 quantifies the frequency of earthquakes of different magnitudes in each region and increasing
 430 stress levels. This leads to a decrease in the b-value and may be associated with large magnitude
 431 earthquakes (Scholz, 2015; Dong et al., 2022). Studies have established a theoretical link between
 432 the b-value and fractal dimension, suggesting that lower b-values correspond to lower D values
 433 and vice versa (Aki, 1981; Venegas-Aravena and Cordaro, 2023b). Specifically, this relationship is
 434 expressed as b - value = $b_M 10^{-r(2-D)}$, where b_M is 2.5 and r is a constant between 10^3 and 10^4 (in

435 this study, r is set to medium value 5000 for simulations). This law is illustrated in Figure 3f. The
436 color map indicates earthquake magnitudes, with blue transparency representing events from M_W
437 3.4 to M_W 6.2, corresponding to a D variation of 1.5. The magnitude variation within this zone is
438 $\Delta M_W \approx 2.8M_W$, while the b-value decrease is $\Delta b \approx 0.2$. Red transparency indicates the same variation
439 of D , but with earthquakes ranging from M_W 7.3 to M_W 8.5, corresponding to a $\Delta M_W \approx 1.2$ and a
440 $\Delta b \approx 1.1$ decrease. The reduction in the rate of change of the b-value with respect to magnitude is
441 clearly displayed in Figure 3g. The blue transparent area emphasizes a region where the absolute
442 value of the b-value remains relatively constant, even as the magnitude of earthquakes fluctuates.
443 It is important to note that a 5-point moving average was applied to the data. This suggests that
444 the b-value is less sensitive to changes when the fault system predominantly generates smaller
445 earthquakes. In contrast, the red transparent area reveals a more pronounced relationship
446 between b-value and magnitude, with the b-value fluctuating more rapidly as the magnitude
447 increases. These results imply that a more abrupt decrease in the b-value is associated with
448 smaller changes in magnitude but, likely, also with changes in fault conditions leading to less
449 chaotic behavior.

450

451

452 **4. A reality check: comparison with seismicity in Southern California**

453 We have already compared our theoretical predictions with the output of dynamic simulations of
454 earthquakes; here we make a reality check with the statistical properties of seismic catalogs.

455 Specifically, we validate the compatibility of the relationship $b\text{-value} = b_M 10^{-r(2-D)}$, between the
456 b-value of the Gutenberg-Richter law and the fractal dimension of faulting. Since it is not possible
457 to directly investigate the fractal properties of faults, we calculate the fractal dimension of
458 hypocenters (hereafter referred as D), which are expected to be distributed within a subset of the
459 fracture network; hence, D is equal or lower than the value for the fault system. Nevertheless,
460 even with different coefficients (b_M and r), the empirical law of the b-value follows the same trend
461 because seismic events are supposed to occur throughout the whole investigated crustal volumes.
462 Thus, we specify that we are not interested either in assessing the true fractal dimension of the
463 networks of faults hosting seismicity (an accurate estimation is not feasible) nor the true fractal
464 dimension of seismic events in their long-term behavior (which would require much longer
465 catalogs than available nowadays and accurate declustering). Here, our goal is just the
466 observational validation of the mathematical relationship $b\text{-value} = b_M 10^{-r(2-D)}$. It requires a high-
467 quality relocated seismic catalog produced by a roughly uniformly distributed network of seismic
468 stations (i.e., uniform completeness magnitude). Both the background and triggered components
469 are considered, otherwise the spatial variations of the b-value and fractal dimension vanish
470 preventing any investigation of their relationship with the available catalogs.

471

472

473

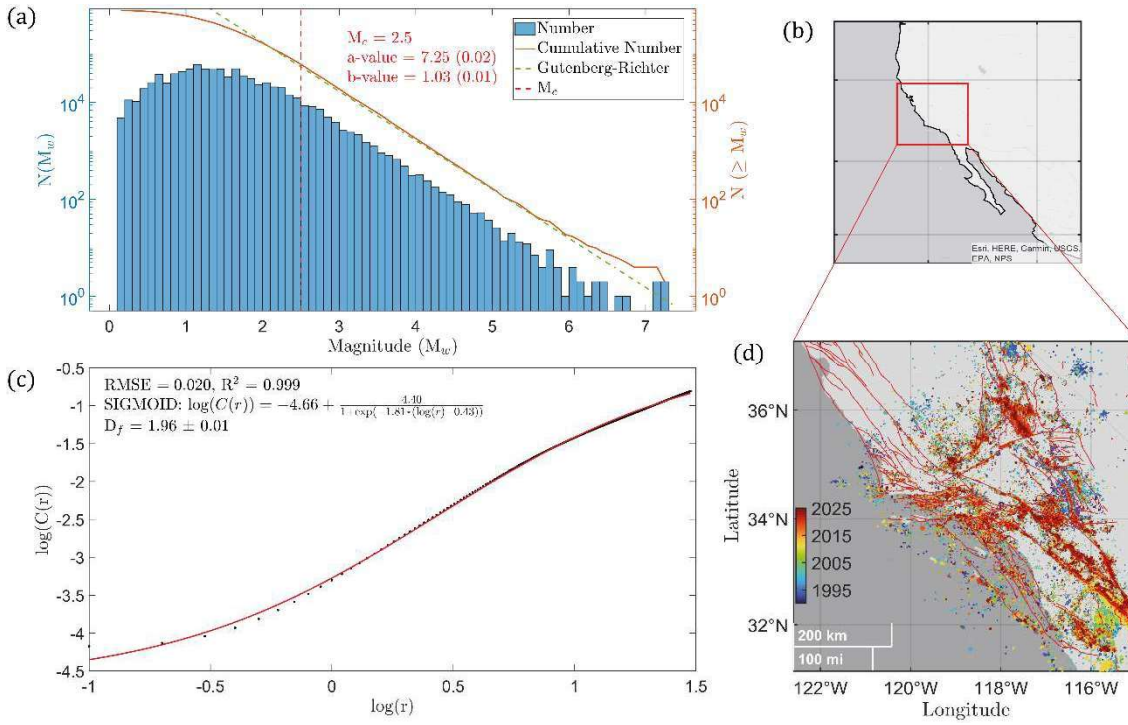
474

475

476

477

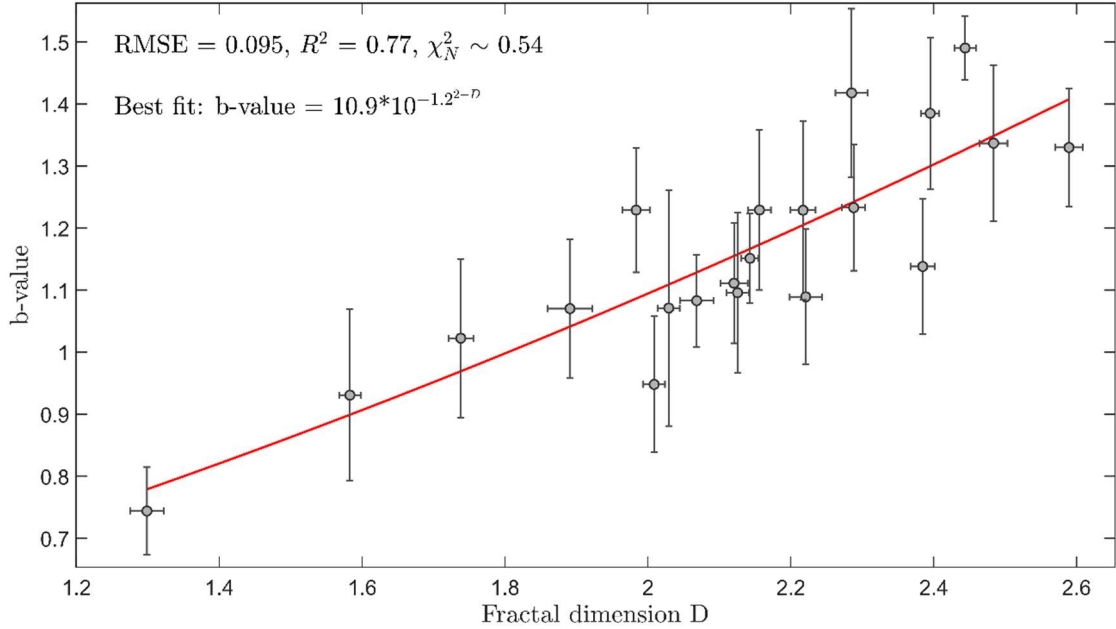
478



479
 480 **Figure 4: Seismicity in Southern California (SEEC Catalog, 1990-2025, latitude 31°-37° N,**
 481 **longitude 115°-122° W, depth lower than 30 km). (a) Frequency-magnitude distribution of**
 482 **seismicity, the completeness magnitude is highlighted by the red vertical dashed line. In (b) and**
 483 **(d) is the map with the spatial distribution of seismicity. (c) log-log representation of the**
 484 **correlation function vs the threshold radial distance (km). The plot shows a range of scales**
 485 **where the curve is well approximated by a line, i.e., hypocenters follow a fractal distribution in**
 486 **space.**

487
 488 We analyze the shallow crustal seismicity (depth lower than 30 km) in Southern California between
 489 1/1/1990 and 20/1/2025 listed in the Waveform Relocated Earthquake Catalog for Southern
 490 California (Hauksson et al., 2012). A visual representation of seismicity considered in this study is
 491 given in Figure 4a, b and d. The catalog is divided into several squared regions. The number and
 492 selection procedure used to define the structure of the subsets do not significantly affect the final
 493 output provided that the fractal probability and the b-value are investigated only for regions with
 494 at least 500 events to get stable and reliable results. Only events above the completeness
 495 magnitude are considered, with $M_c = 2.5$. It is estimated according to the EMR method (Woessner
 496 and Wiemer, 2005). Since short-term aftershocks incompleteness (STAI) after the occurrence of
 497 major events is still present even if a great part of the catalog contains reliable information, the b-
 498 value is calculated using the b-positive algorithm (van der Elst, 2021) with the b-more positive
 499 correction (Lippiello and Petrillo, 2024) to avoid bias. The uncertainty of the b-value is found using
 500 bootstrapping over 100 simulations with acceptance probability equal to 0.5. The fractal dimension
 501 of the hypocenters is measured using the Grassberger and Procaccia algorithm (Grassberger and
 502 Procaccia, 1983). Here, we introduce a new method to remove possible sources of bias in its
 503 estimation due to the arbitrary selection of the lower and upper cut-offs for the linear region in the
 504 log-log plot. The curve of the correlation function $C(r)$ as a function of the threshold radius r is
 505 fitted using the sigmoid function $y = y_0 + k / (1 + e^{-\beta x})$, where $y = \log(C(r))$ and $x = \log(r)$,
 506 while k , β and y_0 are left as free parameters, so that the fractal dimension (i.e., the derivative of
 507 the sigmoid in its symmetry saddle point) is given by $D = k\beta/4$. The uncertainty is calculated by
 508 propagating the fit errors of k and β . The estimation of the fractal dimension of hypocenters for

509 the whole catalog is in Figure 4c. The analysis performed over a wide range of possible grids (both
 510 uniformly spaced and nested according to the number of seismic events within them) shows that
 511 the b-value and the fractal dimension of hypocenters are positively correlated. To improve the
 512 reliability of the result, we only consider subregions in the grid containing at least 500 events
 513 above the completeness magnitude. Moreover, the curve $b\text{-value} = b_M 10^{-r(2-D)}$ provides a good
 514 fit of the relationship between b and D , in agreement with our model. The output of our
 515 investigation is summarized in Figure 5. In this plot, we use a uniformly spaced 50x50 grid.
 516



517
 518 **Figure 5: b-value vs fractal dimension of hypocenters (D) in Southern California. The b-value of**
 519 **the Gutenberg-Richter law is found to be positively correlated with the fractal dimension of**
 520 **hypocenters in Southern California (SCEC Catalog, Hauksson et al., 2012) coherently with**
 521 **previous literature on the topic. The plot represents shallow crustal seismicity from 1/1/1990 to**
 522 **20/1/2025 (depth lower than 30 km) in between latitude 31° - 37° N and longitude 115° - 122° W**
 523 **and above the completeness magnitude $M_c = 2.5$. Error bars represent 2σ uncertainty. The b-**
 524 **value is estimated using the b-more-positive approach, while the fractal dimension of**
 525 **hypocenters is found by applying the Grassberger & Procaccia algorithm (Grassberger and**
 526 **Procaccia, 1983). The red line is the output of the non-linear fit $b\text{-value} = b_M 10^{-r^{2-D}}$ whose**
 527 **trend is predicted in our model and derived in Venegas-Aravena and Cordaro, 2023b.**
 528
 529

530 5. Discussions

531 5.1 The chaotic nature of earthquakes

532 The chaotic nature of earthquakes has been a subject of intense debate within the scientific
 533 community (e.g., Scholz, 1990; Huang and Turcotte, 1992; Goltz, 1997; Vieira, 1999; Yilmaz et al.,
 534 2023). Traditionally, earthquakes have been considered highly unpredictable due to the complexity
 535 of the processes involved in fault rupture (e.g., Geller et al., 1997; Kagan 1997). However, a
 536 growing body of research, spanning conceptual frameworks, crustal stress, thermodynamics,
 537 artificial intelligence, and GNSS measurements, suggests that fault stability may be investigated,
 538 with a potential influence on precursory activity, may be achieved (e.g., Wyss, 1997; Crampin and
 539 Gao, 2010; Posadas et al., 2021; Bhatia et al., 2023; Bletery and Nocquet 2023; Devi et al., 2024),

540 especially in the case of larger magnitude seismic event (Kaveh et al., 2024). In this study, we
541 propose a novel perspective, grounded in multi-scale thermodynamics, suggesting that the chaotic
542 nature of earthquakes may be modulated by the residual energy stored within faults volumes
543 (Venegas-Aravena and Cordaro 2023a). These primarily theoretical developments suggest that as
544 the thermodynamic fractal dimension (D) decreases, the residual energy in the system increases.
545 This correlation is further supported by the framework presented in Section 2, where we
546 demonstrate that a higher residual energy is linked to a lower sum of Lyapunov exponents Λ (red
547 regions in Figure 1b), a hallmark of reduced chaoticity. Consequently, earthquakes with higher
548 residual energy exhibit more deterministic behavior, as larger magnitude earthquakes (lower Λ)
549 show a smaller change in magnitude per unit of residual energy (Figure 1c). This suggests that
550 these earthquakes are less susceptible to the exponential growth of small perturbations, a
551 hallmark of chaotic systems. Figure 1c presents the analysis of $\Delta M_W/E^{res}$, revealing an interesting
552 parallelism with the findings of Kanamori and Rivera (2004). In their study, they defined the ratio
553 E_R/M_0 , which is associated with the radiative efficiency of an earthquake, representing the
554 fraction of energy released during rupture that is radiated as seismic waves. Their results indicated
555 that this ratio increases with earthquake size, suggesting proportionally greater radiated energy for
556 larger magnitude events. In this regard, both the work of Kanamori and Rivera (2004) and the
557 present study (Figure 1c) imply a scale-dependent behavior of earthquakes, where larger events
558 exhibit different characteristics concerning the role of energy in the rupture and radiation
559 processes compared to smaller ones. However, this study focuses on the change in sensitivity
560 Σ ($\Sigma = \Delta M_W/E^{res}$) of a fault to a perturbation, whereas Kanamori and Rivera (2004) investigated
561 the radiative efficiency ε ($\varepsilon = E_R/M_0$). Abstracting from the evident unit discrepancies, a potential
562 compatibility between these findings can be inferred by positing an inverse relationship between
563 seismic sensitivity and radiative efficiency, such that higher efficiency corresponds to a system less
564 sensitive to initial perturbations. This hypothetical relationship can be expressed as:

$$565 \quad \Sigma = \frac{\varepsilon_0}{\varepsilon} \quad (6)$$

566 where ε_0 represents a quantity with the necessary physical units to establish the equality of the
567 Equation. Despite this, more analyses need to be done in order to establish a deeper
568 understanding between sensibility and efficiency. Section 3 evaluates the proposed hypothesis
569 through numerical simulations of kinematic rupture using the HE-B method. This method has been
570 effective in modeling self-arrested earthquakes that comply with observational constraints, such as
571 the asperity criterion of Somerville et al. (1999), which links the zone of high slip (known as
572 asperity) to the release of a large amount of seismic energy. The results obtained show a clear
573 relationship between residual energy and the variability in earthquake magnitude. For instance,
574 the blue zone in Figure 2e demonstrates that smaller earthquakes ($M_W < 6.6$) exhibit a high
575 sensitivity to variations in available energy. This means that small increases in available energy can
576 lead to significant increases in the magnitude of the resulting earthquake, as evidenced by the high
577 values of ΔM_W and the regions of high magnitude variability (transparent blue zone in Figure 2f).
578 Specifically, this indicates that a 1% increase in available energy can result in an increase in the
579 magnitude of the resulting earthquake greater than $0.5M_W$. In other words, when a fault has a
580 specific low value of available energy (e.g., $0.1 \times 10^7 J/m^2$) and has the potential to generate a
581 magnitude $M_W = 5$ earthquake, it can produce a larger earthquake ($M_W = 5.5$) or a smaller one (M_W
582 $= 4.5$) if the available energy is slightly increased or decreased. In contrast, larger earthquakes
583 ($M_W > 7.8$) show a notable lack of sensitivity to changes in available energy (transparent green and
584 red zones in Figure 2f). These zones indicate that a slight increase or decrease in available energy
585 does not produce significant changes in the magnitude of the resulting earthquake. This low
586 sensitivity demonstrates less chaotic behavior in the simulations, where larger earthquakes are

587 more predictable and less influenced by small perturbations. This also suggests that these larger
588 events may also be more predictable. In line with this, analyses conducted in seismic rupture
589 simulations with a rate-and-state friction law on simple faults (Kaveh et al., 2024) are consistent
590 with the results shown in this work, which is based on the distribution of residual energy. An
591 interesting aspect of the work by Kaveh et al. (2024) comes from the threshold above which
592 predictions can be made. They observed that it was possible to make forecasts of earthquakes with
593 magnitudes greater than approximately $M_W 6.9$. In contrast, Figures 2e and 2f indicate that the
594 variation in magnitude due to a change in available energy begins to be less than $0.1M_W$ when
595 earthquakes begin to have magnitudes greater than $M_W 6.6$ (transparent yellow zone). This
596 suggests a similar threshold for predictability in both studies.

597

598 **5.2 Insights from numerical simulations**

599 To further assess the link between residual energy and chaos in seismic activity, numerical
600 simulations were performed varying both the fracture energy distribution and the system's
601 available energy, in accordance with Equation 5. The findings strongly corroborate the proposed
602 hypothesis. Figure 3c, for example, demonstrates an excellent agreement between the simulated
603 magnitude-parameter D relationship (black curve) and the theoretically predicted one (Equation 2,
604 red curve), affirming the established theoretical connection between parameter D , residual energy,
605 and simulated earthquake magnitudes. Additionally, Figures 3d and 3e corroborate the trend
606 observed in the earthquakes of Figure 2: larger magnitude earthquakes exhibit a smaller variation
607 in their magnitude, suggesting a lower degree of chaos in these events. To gain further credibility, a
608 parameter more commonly used in seismology was needed. The b-value of the Gutenberg-Richter
609 law has traditionally been used as an indicator of the relative occurrence rate of earthquakes of
610 different magnitudes (Ito and Kaneko, 2023; Lacidogna et al., 2023). In this study, the relationship
611 between the b-value and the degree of chaos in seismicity has been explored. In particular, Figure
612 3f shows that the b-value decreases more abruptly for earthquakes with magnitudes greater than
613 $M_W 7.3$ (red zone), indicating a decrease in the occurrence rate of smaller earthquakes relative to
614 larger ones. This behavior is associated with b-value changes on the order of 0.4 and suggests a
615 less chaotic regime. On the other hand, for earthquakes with magnitudes less than $M_W 6.3$ (blue
616 zone), the b-value exhibits less pronounced changes, indicating a greater variability in the
617 occurrence rate of earthquakes of different magnitudes, and therefore, a more chaotic regime.
618 This relationship between the b-value and seismic chaos is consistent with the interpretation of
619 parameter D . Low D values (associated with higher-magnitude earthquakes) imply a more
620 homogeneous distribution of residual energy over a larger area within faults, thereby reducing the
621 probability and number of smaller events. Consequently, the ratio of large to small events, known
622 as the b-value, is directly influenced by D . Therefore, it can be argued that a typical decrease in the
623 b-value (e.g., Rivière et al., 2018; Sharon et al., 2022; Chan et al., 2024) is a measure of the chaos
624 of a system, supporting the notion that low b-values are associated with imminent larger
625 magnitude earthquakes, coherently with previous research (e.g., Gulia and Wiemer, 2019).

626

627 **5.3 Implications of our new relationship between b-value and fractal dimension and comparison** 628 **with previous observations**

629 We also prove the theoretical relationship between the b-value and fractal dimension $b\text{-value} =$
630 $b_M 10^{-r(2-D)}$, also supporting the idea that large earthquakes tend to occur within networks with
631 low fractal dimensions (i.e., along major faults). See Figure 5 for the output in the case of the SCEC
632 Catalog in Southern California (1990-2025). Observations show good agreement with theory and,
633 even though with relatively large uncertainties, are statistically robust. It is important to note that,

634 according to Venegas-Aravena and Cordaro (2023b), the case where b-value and D are
635 approximately proportional can be obtained, as shown in Figure 5. The direct effect of the fractal
636 dimension of faulting on the maximum magnitude is more difficult to observe since large
637 earthquakes are rare events and the available seismic catalogs only contain a few cases, if any, of
638 events with the largest expected magnitude for each fault system, preventing a reliable analysis.
639 Moreover, the results would be rescaled for the size of the largest seismogenic source in each fault
640 network, which is tricky to estimate. Conversely, the b-value can nowadays be evaluated by robust
641 and unbiased estimators. This is the reason why we choose to validate directly the relationship
642 between b and D .

643
644 Our finding that an increase in b corresponds to an increase in D implies that regions with more
645 frequent small earthquakes (higher b-value) also exhibit more spatially diffuse seismicity, whereas
646 areas dominated by larger events (lower b-value) display tighter hypocenter clustering.
647 This relationship is not an unprecedented result, and it is consistent with previous studies that
648 have linked stress heterogeneity to both earthquake size distribution and spatial patterns. Among
649 them, Hirata (1989) demonstrated that fault network complexity influences seismicity clustering,
650 suggesting that structural heterogeneity affects both the b-value and hypocenter distributions.
651 Wiemer & Wyss (1997) further established that the spatial variations in b-value reflect differences
652 in stress regimes, with lower b-values often found in high-stress zones where earthquakes may
653 nucleate along preferential fault planes, leading to stronger clustering (lower D). Nanjo et al. (1998)
654 provided direct evidence that higher b-values correlate with more uniformly distributed seismicity,
655 supporting our observed positive b-value- D correlation. While Tormann et al. (2014) argued that
656 regions with homogeneous stress conditions (higher b-value) tend to produce less clustered
657 seismicity, reinforcing the idea that stress state modulates both earthquake size and spatial
658 organization. Finally, Zaccagnino and Doglioni (2022) showed that the fractal properties of faulting
659 affect the earthquake rupture processes that, in turn, reveal themselves as different scaling
660 exponents of the Gutenberg-Richter law. The new advance here is that our mathematical
661 derivation allows us to relate fractal dimension and scaling properties of seismicity in the
662 framework of dynamical systems and chaos theory. These findings, together with previous
663 observational ones, underscore the importance of structural heterogeneity in governing both the
664 frequency-magnitude distribution and the spatial complexity of seismicity as well as its chaotic
665 properties, offering a unified framework for interpreting earthquake dynamical patterns.

666 667 **5.4 Impact on the predictability of larger events**

668 The analyses conducted in this study, which involves theoretical, numerical and observational data,
669 contrast with the traditional view of earthquakes as highly chaotic systems. However, it is
670 important to note that our proposal does not dismiss the role of chaos in seismic rupture dynamics.
671 Rather, it suggests that the chaotic behavior may be modulated by the amount of residual energy
672 stored in the fault. In other words, when residual energy is high, the probability of releasing all that
673 energy in a sudden event increases due to the coalescence of different fault segments ready to
674 nucleate or that can be dynamically activated during the coseismic phase. Conversely, when
675 residual energy is low, the fault has more options for releasing that energy, which can lead to
676 seismic ruptures of varying sizes. Our findings have significant implications for understanding the
677 precursor seismicity, known as foreshocks (e.g., Lippiello et al., 2019; Bolton et al., 2023). If we can
678 accurately quantify the residual energy in a fault, we may be able to estimate the probability of
679 large magnitude earthquakes and assess their destructive potential.

680

681 This is particularly significant as recent research indicates that approximately half of large-
682 magnitude seismic events may be preceded by precursor seismic activity, although the magnitude
683 difference between foreshocks and mainshocks does not appear to be substantial (Wetzler et al.,
684 2023). This suggests that states of higher energy preferentially evolve into large earthquakes.
685 These states are associated with a greater amount of available energy, which is directly related to
686 stress. Here, it is important to note that low values of D also indicate an accumulation of stress in
687 localized areas (Venegas-Aravena et al., 2022). Geodetic measurements have confirmed this
688 accumulation of localized stresses between earthquakes of magnitudes greater than $M_W 7$ (Kato
689 and Ben-Zion, 2020). Additionally, foreshocks also appear to be related to the geometric conditions
690 of faults (e.g., McLaskey and Kilgore, 2013; Cattania and Segall, 2021), which can be incorporated
691 into the residual energy through fracture energy. Subsequently, residual energy can be used to
692 estimate the physics of seismic precursors. For instance, it has been estimated that foreshocks may
693 not be reliable when estimating the probability of subsequent mainshocks (Zaccagnino et al.,
694 2024). Here, residual energy in the context of multi-scale thermodynamics can offer two
695 explanations for the lack of clarity regarding foreshocks. Firstly, foreshock-type activity should arise
696 as a stress perturbation, which, when considering a state of residual energy, can trigger events of
697 different magnitudes but within a range of magnitudes close to that of the potential future
698 mainshock. However, the magnitude of these foreshocks can be chaotic, limiting the ability to
699 conduct statistical analyses and thus declaring them as foreshocks in real-time measurements.
700 Secondly, the increase in residual energy implies a lower variability in the magnitude of
701 earthquakes, in agreement with Lippiello et al., 2024. This suggests that when residual energy may
702 be very high in a fault, stress perturbation has higher chances to trigger large earthquakes, limiting
703 the existence of foreshocks. That is, the probability that larger earthquakes are affected or
704 associated with foreshocks could decrease with an increase in the magnitude of the mainshock.
705 Here, one way to associate foreshocks with large magnitude mainshocks is if the rupture area of a
706 foreshock reaches a zone of the fault with very high residual energy, which could be seen as a
707 perturbation leading to a single large subsequent earthquake. This scenario could occur in the so-
708 called "Mogi Doughnut" of subduction zones (Mogi, 1969), where the shallowest zones of the plate
709 interface accumulate large amounts of energy while most seismicity occurs at deeper locations
710 with lower accumulated energy (Schurr et al., 2020).

711
712 The findings and interpretation carried out in this work agree with recent modeling and
713 observational findings in the literature (e.g., Nielsen, 2024) and could also influence future
714 research, which may focus on developing methods to directly measure residual energy in natural
715 faults, creating more sophisticated models that incorporate parameter D and allow for the
716 simulation of the evolution of residual energy over time. Finally, exploring the implications of our
717 results for seismic risk assessment and the design of earthquake-resistant structures.

718

719 **5.5. Limitations of our model, challenges and future directions**

720 While the dynamical framework presented in this study offers insights into earthquake
721 predictability through chaos theory and thermodynamics, several limitations must be
722 acknowledged. We list them hereafter:

- 723 1) Earthquakes emerge from spatially extended, heterogeneous systems where stress
724 interactions, geometric complexities, and multiscale processes challenge deterministic
725 models. Our framework suggests reduced chaoticity for large events essentially promoted
726 by the control of the residual energy on the final size of the mainshock. This result is in
727 conflict with self-organized criticality (SOC) (Bak and Tang, 1989), which argues that scale-

728 invariant earthquake statistics arise from stochastic processes under critical conditions
729 rather than deterministic chaos. Conversely, our model is consistent with recent results
730 suggesting that seismicity usually operates well below criticality and that large earthquakes
731 show special features different from smaller ones which make them more predictable
732 (Sornette, 2009; Sornette and Ouillon, 2012; Nandan et al., 2021).

733 2) The link between Lyapunov exponents (Λ), residual energy, and predictability relies on
734 numerical simulations (e.g., HE-B method) with idealized friction laws and boundary
735 conditions. Real faults also exhibit complicated friction laws, off-fault plasticity, and long-
736 range interactions which are challenging to be fully incorporated.

737 3) The proposed predictability threshold (M 6.6-6.9) agrees with Kaveh et al. (2024), but
738 universal applications remain uncertain. Regional variations in fault maturity, stress
739 accumulation, and tectonic setting may modulate chaotic behavior, limiting generalizations.

740 4) Empirical validation relies on seismic catalogs with incomplete records of large events (due
741 to their rarity) and potential biases in b -value and fractal dimension estimation. While
742 Southern California catalog supports our $b - D$ positive correlation, global applicability
743 requires testing across diverse tectonic regimes.

744

745 **6. Conclusions**

746 The results obtained in this study suggest that the chaotic behavior of earthquakes can be
747 modulated by the amount of residual energy stored in the fault. Our findings indicate that larger
748 earthquakes, associated with higher residual energy, exhibit less chaotic behavior. This new
749 perspective challenges traditional conceptions about the nature of earthquakes and opens new
750 avenues of research in seismology. While these results are promising, further research is required
751 to confirm and deepen our findings. Specifically, methods need to be developed to directly
752 measure residual energy in natural faults and to construct more sophisticated models that
753 incorporate the parameter D . Indeed, our approach advances a deterministic perspective on large
754 earthquakes, even though limitations highlight the need for more advanced models combining
755 chaos theory and statistical seismology. Future works should address multiscale fault physics and
756 observational uncertainties to refine our predictive framework. This research will allow us to
757 advance our understanding of the mechanisms governing the generation and propagation of
758 earthquakes and pave the way for a better assessment and mitigation of seismic risk.

759

760 **Data and Code Availability**

761 Data and codes are available upon reasonable requests to both the authors.

762

763 **Acknowledgment**

764 The authors wish to thank the editor Giuseppe Petrillo for handling the manuscript and two
765 anonymous reviewers whose comments and suggestions greatly improved the first version of the
766 paper. Discussions with Valeria Becerra-Carreño, Enrique G. Cordaro, Matteo Picozzi and Didier
767 Sornette have been inspiring for the work.

768

769 **Competing interests**

770 The authors declare no competing interests.

771

772 **References**

773 Aki K (1981) A probabilistic synthesis of precursory phenomena, in Earthquake Prediction: An
774 International Review, pp. 566–574, eds Simpson D.W. Richards P. G., AGU, Washington, DC

775
776 Aksoy CG, Chupilkin M, Koczan Z, Plekhanov A (2024) Unearthing the impact of earthquakes: A
777 review of economic and social consequences. *Journal of Policy Analysis and Management* 2024(1):
778 1-22. <https://doi.org/10.1002/pam.22642>
779
780 Bak P, Tang C (1989) Earthquakes as a self-organized critical phenomenon. *Journal of Geophysical*
781 *Research: Solid Earth*, 94(B11), 15635-15637. <https://doi.org/10.1029/JB094iB11p15635>.
782
783 Barras F, Thøgersen K, Aharonov E, Renard F (2023) How Do Earthquakes Stop? Insights From a
784 Minimal Model of Frictional Rupture. *Journal of Geophysical Research* 128(8): 1-22.
785 <https://doi.org/10.1029/2022JB026070>
786
787 Bhatia M, Ahanger TA, Manocha A (2023) Artificial intelligence based real-time earthquake
788 prediction. *Engineering Applications of Artificial Intelligence* 120(1):1-14.
789 <https://doi.org/10.1016/j.engappai.2023.105856>
790
791 Bletery Q, J-M Nocquet (2023) The precursory phase of large earthquakes. *Science* 381(6655): 297-
792 301. <https://doi.org/10.1126/science.adg2565>
793
794 Bolton DC, Marone C, Saffer D, Trugman DT (2023) Foreshock properties illuminate nucleation
795 processes of slow and fast laboratory earthquakes. *Nature Communications* 14(3859): 1-11.
796 <https://doi.org/10.1038/s41467-023-39399-0>
797
798 Cattania C, Segall P (2021) Precursory Slow Slip and Foreshocks on Rough Faults. *Journal of*
799 *Geophysical Research* 126(4): 1-20. <https://doi.org/10.1029/2020JB020430>
800
801 Chan C-H, Kao J-C, Chen D-Y (2024) Spatial–temporal variations of b-values prior to medium-to-
802 large earthquakes in Taiwan and the feasibility of real-time precursor monitoring. *Earth Planets*
803 *Space* 76(119): 1-14. <https://doi.org/10.1186/s40623-024-02065-w>
804
805 Chen Y, Yang H (2016) Numerical simulation and pattern characterization of nonlinear
806 spatiotemporal dynamics on fractal surfaces for the whole-heart modeling applications. *The*
807 *European Physical Journal B* 89(181): 1-16. <https://doi.org/10.1140/epjb/e2016-60960-6>
808
809 Christensen DH, Beck SL (1994) The rupture process and tectonic implications of the great 1964
810 Prince William Sound earthquake. *Pure and Applied Geophysics* 142(1): 29–53.
811 <https://doi.org/10.1007/BF00875967>
812
813 Colavitti L, Lanzano G, Sgobba S, Pacor F, Gallovič F (2022) Empirical Evidence of Frequency-
814 Dependent Directivity Effects From Small-To-Moderate Normal Fault Earthquakes in Central Italy.
815 *Journal of Geophysical Research* 127(6):1-24. <https://doi.org/10.1029/2021JB023498>
816
817 Crampin S, Gao Y (2010) Earthquakes can be stress-forecast. *Geophysical Journal International*
818 180(3):1124–1127. <https://doi.org/10.1111/j.1365-246X.2009.04475.x>
819

820 Devi DR, Govindarajan P, Venkatanathan N (2024) Towards real-time earthquake forecasting in
821 Chile: Integrating intelligent technologies and machine learning. *Computers and Electrical*
822 *Engineering* 117(1):1-15. <https://doi.org/10.1016/j.compeleceng.2024.109285>
823

824 Dong L, Zhang L, Liu H, Diu K, Liu X (2022) Acoustic Emission b Value Characteristics of Granite
825 under True Triaxial Stress. *Mathematics* 10(3):1-16. <https://doi.org/10.3390/math10030451>
826

827 Eden A, Foias C, Temam R (1991) Local and Global Lyapunov exponents. *Journal of Dynamics and*
828 *Differential Equations* 3(1): 133–177. <https://doi.org/10.1007/BF01049491>
829

830 Erickson BA, Birnir B, Lavallée D (2011) Periodicity, chaos and localization in a Burridge–Knopoff
831 model of an earthquake with rate-and-state friction. *Geophysical Journal International* 187(1):
832 178–198. <https://doi.org/10.1111/j.1365-246X.2011.05123.x>
833

834 Geller RJ, Jackson DD, Kagan YY, Mulargia F (1997) Earthquakes Cannot Be Predicted. *Science*
835 275(5306): 1616-1617. <https://doi.org/10.1126/science.275.5306.1616>
836

837 Goltz C (1997) Fractal and Chaotic Properties of Earthquakes. *Lecture Notes in Earth Sciences* 77(1):
838 3-164. <https://doi.org/10.1007/BFb0028316>
839

840 Grassberger P, Procaccia I (1983) Measuring the strangeness of strange attractors. *Physica D:*
841 *nonlinear phenomena* 9(1-2):189-208. [https://doi.org/10.1016/0167-2789\(83\)90298-1](https://doi.org/10.1016/0167-2789(83)90298-1)
842

843 Gualandi A, Faranda D, Marone C, Cocco M, Mengaldo G (2023) Deterministic and stochastic chaos
844 characterize laboratory earthquakes. *Earth and Planetary Science Letters* 604(1): 1-13.
845 <https://doi.org/10.1016/j.epsl.2023.117995>
846

847 Gudmundsson A (2014) Elastic energy release in great earthquakes and eruptions. *Frontiers in*
848 *Earth Science* 2(1):1-12. <https://doi.org/10.3389/feart.2014.00010>
849

850 Gulia L, Wiemer S (2019) Real-time discrimination of earthquake foreshocks and aftershocks.
851 *Nature*, 574(7777), 193-199. <https://doi.org/10.1038/s41586-019-1606-4>
852

853 Hauksson E, Yang W, Shearer PM (2012) Waveform relocated earthquake catalog for southern
854 California (1981 to June 2011). *Bulletin of the Seismological Society of America*, 102(5), 2239-2244.
855 <https://doi.org/10.1785/0120120010>
856

857 Hirata T (1989) A correlation between the b value and the fractal dimension of earthquakes.
858 *Journal of Geophysical Research: Solid Earth*, 94(B6), 7507-7514.
859 <https://doi.org/10.1029/JB094iB06p07507>
860

861 Hoover WG, Posch HA (1994) Second-law irreversibility and phase-space dimensionality loss from
862 time-reversible nonequilibrium steady-state Lyapunov spectra. *Physical Review E* 49(3):1913-1921.
863 <https://doi.org/10.1103/PhysRevE.49.1913>
864

865 Huang J, Turcotte DL (1990) Are earthquakes an example of deterministic chaos? *Geophysical*
866 *Research Letters* 17(3):223-226. <https://doi.org/10.1029/GL017i003p00223>

867
868 Huang SL, Oelfke SM, Speck RC (1992) Applicability of fractal characterization and modelling to
869 rock joint profiles. *International Journal of Rock Mechanics and Mining Sciences & Geomechanics*
870 *Abstracts* 29(2):89-98. [https://doi.org/10.1016/0148-9062\(92\)92120-2](https://doi.org/10.1016/0148-9062(92)92120-2)
871
872 Huang J, Turcotte DL (1992) Chaotic seismic faulting with a mass-spring model and velocity-
873 weakening friction. *Pure and Applied Geophysics* 138(1): 569–589.
874 <https://doi.org/10.1007/BF00876339>
875
876 Iaccarino AG, Picozzi M (2023) Detecting the Preparatory Phase of Induced Earthquakes at The
877 Geysers (California) Using K-Means Clustering. *Journal of Geophysical Research* 128(10): 1-18.
878 <https://doi.org/10.1029/2023JB026429>
879
880 Ito R, Kaneko Y (2023) Physical Mechanism for a Temporal Decrease of the Gutenberg-Richter b-
881 Value Prior to a Large Earthquake. *Journal of Geophysical Research* 128(12):1-21.
882 <https://doi.org/10.1029/2023JB027413>
883
884 Kagan YY (1991) Fractal dimension of brittle fracture. *Journal of Nonlinear Science* 1(1):1-16.
885 <https://doi.org/10.1007/BF01209146>
886
887 Kahandawa KARVD, Domingo ND, Park KS (2018) Earthquake damage estimation systems:
888 Literature review. *Procedia Engineering* 212(1): 622-628.
889 <https://doi.org/10.1016/j.proeng.2018.01.080>
890
891 Kanamori H, Rivera L (2004) Static and Dynamic Scaling Relations for Earthquakes and Their
892 Implications for Rupture Speed and Stress Drop. *Bulletin of the Seismological Society of America*
893 94(1): 314–319. <https://doi.org/10.1785/0120030159>
894
895 Kato A, Ben-Zion Y (2020) The generation of large earthquakes. *Nature Reviews Earth &*
896 *Environment* 2(1): 26–39. <https://doi.org/10.1038/s43017-020-00108-w>
897
898 Kintner JA, Ammon CJ, Cleveland KM, Herman M (2018) Rupture processes of the 2013–2014
899 Minab earthquake sequence, Iran. *Geophysical Journal International* 213(3): 1898–1911.
900 <https://doi.org/10.1093/gji/ggy085>
901
902 Kagan YY (1997) Are earthquakes predictable? *Geophysical Journal International* 131(3): 505–525.
903 <https://doi.org/10.1111/j.1365-246X.1997.tb06595.x>
904
905 Kaveh H, Avouac JP, Stuart AM (2024) Spatiotemporal forecast of extreme events in a chaotic
906 dynamical model of slow slip events. *Geophysical Journal International*, ggae417.
907 <https://doi.org/10.1093/gji/ggae417>
908
909 Knopoff L (1958) Energy Release in Earthquakes. *Geophysical Journal International* 1(1): 44–52.
910 <https://doi.org/10.1111/j.1365-246X.1958.tb00033.x>
911

912 Lacidogna G, Borla O, De Marchi V (2023) Statistical Seismic Analysis by b-Value and Occurrence
913 Time of the Latest Earthquakes in Italy. *Remote Sensing* 15(21):1-20.
914 <https://doi.org/10.3390/rs15215236>
915

916 Leonard M (2010) Earthquake Fault Scaling: Self-Consistent Relating of Rupture Length, Width,
917 Average Displacement, and Moment Release. *Bulletin of the Seismological Society of America*
918 100(5A): 1971–1988. <https://doi.org/10.1785/0120090189>
919

920 Li Q, Sun J, Xi G, Liu J (2022) The Doppler effect induced by earthquakes: A case study of the
921 Wenchuan MS8.0 earthquake. *Geodesy and Geodynamics* 13(5): 435-444.
922 <https://doi.org/10.1016/j.geog.2021.12.006>
923

924 Lippiello E, de Arcangelis L, Godano C (2024) Positive Answer on the Existence of Correlations
925 between Positive Earthquake Magnitude Differences. *Physical Review Letters* 133(24): 244101.
926 <https://doi.org/10.1103/PhysRevLett.133.244101>.
927

928 Lippiello E, Godano C, de Arcangelis L (2019) The Relevance of Foreshocks in Earthquake Triggering:
929 A Statistical Study. *Entropy* 21(2): 1-13. <https://doi.org/10.3390/e21020173>
930

931 Lippiello E, Petrillo G (2024) b-more-incomplete and b-more-positive: Insights on a robust
932 estimator of magnitude distribution. *Journal of Geophysical Research: Solid Earth*, 129(2),
933 e2023JB027849. <https://doi.org/10.1029/2023JB027849>
934

935 Martínez-Lopez MR (2023) Study of the rupture processes of the 1989 (Mw 6.9) and 2021 (Mw 7.0)
936 Guerrero earthquakes using teleseismic records: Seismotectonic implications. *Geologica Acta* 21(9):
937 1-14. <https://doi.org/10.1344/GeologicaActa2023.21.9>
938

939 McLaskey GC, Kilgore BD (2013) Foreshocks during the nucleation of stick-slip instability. *Journal of*
940 *Geophysical Research* 118(6):2982-2997. <https://doi.org/10.1002/jgrb.50232>
941

942 Mogi K (1969) Some features of recent seismic activity in and near Japan (2) activity before and
943 after great earthquakes. *Bulletin of the Earthquake Research Institute* 47(4): 395–417.
944

945 Murase K (2004) A Characteristic Change in Fractal Dimension Prior to the 2003 Tokachi-oki
946 Earthquake (M J = 8.0), Hokkaido, Northern Japan. *Earth, Planets and Space* 56(3): 401–405.
947 <https://doi.org/10.1186/BF03353072>
948

949 Nandan S, Ram S K, Ouillon G, Sornette D (2021) Is seismicity operating at a critical point?. *Physical*
950 *Review Letters*, 126(12), 128501. <https://doi.org/10.1103/PhysRevLett.126.128501>.
951

952 Nanjo KG, Nagahama H, Satomura M (1998) Rates of aftershock decay and the fractal structure of
953 active fault systems. *Geophysical Research Letters*, 25(19), 3677–3680.
954 <https://doi.org/10.1029/98GL02742>
955

956 Nielsen S (2024) Earthquakes big and small: same physics, different boundary conditions. *ArXiv*
957 preprint arXiv:2411.00544. <https://doi.org/10.48550/arXiv.2411.00544>
958

959 Noda A, Saito T, Fukuyama E, Urata Y (2021) Energy-Based Scenarios for Great Thrust-Type
960 Earthquakes in the Nankai Trough Subduction Zone, Southwest Japan, Using an Interseismic Slip-
961 Deficit Model. *Journal of Geophysical Research* 126(5):1-20.
962 <https://doi.org/10.1029/2020JB020417>
963

964 Onsager L (1931a) Reciprocal Relations in Irreversible Processes. I. *Physical Review* 37(1): 405-426.
965 <https://doi.org/10.1103/PhysRev.37.405>
966

967 Onsager L (1931b) Reciprocal Relations in Irreversible Processes. II. *Physical Review* 38(1): 2265-
968 2279. <https://doi.org/10.1103/PhysRev.38.2265>
969

970 Otarola C, Ruiz S, Herrera C, Madariaga R, Siegel C (2021) Dynamic rupture of subduction
971 earthquakes located near the trench. *Earth and Planetary Science Letters* 562(1): 1-12.
972 <https://doi.org/10.1016/j.epsl.2021.116842>
973

974 Padilla AMR, Oskin ME, Brodsky EE, Dascher-Cousineau K, Herrera V, White S (2024) The Influence
975 of Fault Geometrical Complexity on Surface Rupture Length. *Journal of Geophysical Research*
976 51(20):1-10. <https://doi.org/10.1029/2024GL109957>
977

978 Perinelli A, Ricci L, De Santis A, Iuppa R (2024) Earthquakes unveil the global-scale fractality of the
979 lithosphere. *Communications Earth & Environment* 5(146): 1-13. <https://doi.org/10.1038/s43247-023-01174-w>
980

981

982 Pétrélis F, Chanard K, Schubnel A, Hatano T (2021) Earthquake sensitivity to tides and seasons:
983 Theoretical studies. *Journal of Statistical Mechanics: Theory and Experiment*, 2021(2), 023404.
984 <https://doi.org/10.1088/1742-5468/abda29>
985

986 Posadas A, Morales J, Ibañez JM, Posadas-Garzon A (2021) Shaking earth: Non-linear seismic
987 processes and the second law of thermodynamics: A case study from Canterbury (New Zealand)
988 earthquakes. *Chaos, Solitons & Fractals* 151(1): 1-12. <https://doi.org/10.1016/j.chaos.2021.111243>
989

990 Renou J, Vallée M, Aochi H (2022) Deciphering the Origins of Transient Seismic Moment
991 Accelerations by Realistic Dynamic Rupture Simulations. *Bulletin of the Seismological Society of*
992 *America* 112(3): 1240-1251. <https://doi.org/10.1785/0120210221>
993

994 Rivera L, Kanamori H (2005) Representations of the radiated energy in earthquakes. *Geophysical*
995 *Journal International* 162(1):148–155. <https://doi.org/10.1111/j.1365-246X.2005.02648.x>
996

997 Rivière J, Lv Z, Johnson PA, Marone C (2018) Evolution of b-value during the seismic cycle: Insights
998 from laboratory experiments on simulated faults. *Earth and Planetary Science Letters* 482(1): 407-
999 413. <https://doi.org/10.1016/j.epsl.2017.11.036>
1000

1001 Rubinstein JL, La Rocca M, Vidale JE, Creager KC, Wech AG (2008) Tidal modulation of nonvolcanic
1002 tremor. *Science*, 319(5860), 186-189. <https://doi.org/10.1126/science.1150558>
1003

1004 Ruelle D (1983) *Chaotic Evolution and Strange Attractors*; Cambridge University: New York, NY, USA,
1005 1983

1006

1007 Salditch L, Stein S, Neely J, Spencer BD, Brooks EM, Agnon A, Liu M (2020) Earthquake supercycles
 1008 and long-term fault memory. *Tectonophysics*, 774, 228289.
 1009 <https://doi.org/10.1016/j.tecto.2019.228289>

1010

1011 Scholz CH (1990) Earthquakes as chaos. *Nature* 348(1): 197–198.
 1012 <https://doi.org/10.1038/348197a0>

1013

1014 Scholz CH (2015) On the stress dependence of the earthquake b value. *Geophysical Research
 1015 Letters* 42(5):1399-1402. <https://doi.org/10.1002/2014GL062863>

1016

1017 Schurr B, Moreno M, Tréhu AM, Bedford J, Kummerow J, Li S, Oncken O (2020) Forming a Mogi
 1018 Doughnut in the Years Prior to and Immediately Before the 2014 M8.1 Iquique, Northern Chile,
 1019 Earthquake. *Geophysical Research Letters* 47(16): 1-10. <https://doi.org/10.1029/2020GL088351>

1020

1021 Sharon M, Kurzon I, Wetzler N, Sagy A, Marco S, Ben-Avraham Z (2022) Variations of the seismic b-
 1022 value along the Dead Sea transform. *Frontiers in Earth Science* 10(1): 1-19.
 1023 <https://doi.org/10.3389/feart.2022.1074729>

1024

1025 Silverio-Murillo A, Balmori-de-la-Miyar J, Sobrino F, Prudencio D (2024) Do earthquakes increase or
 1026 decrease crime? *World Development* 182(1): 1-8. <https://doi.org/10.1016/j.worlddev.2024.106711>

1027

1028 Somerville P, Irikura K, Graves R, Sawada S, Wald D, Abrahamson N, Iwasaki Y, Kagawa T, Smith N,
 1029 Kowada A (1999) Characterizing crustal earthquake slip models for the prediction of strong ground
 1030 motion. *Seismological Research Letters* 70(1): 59–80. <https://doi.org/10.1785/gssrl.70.1.59>

1031

1032 Sornette D (2009) Dragon-kings, black swans and the prediction of crises. arXiv preprint
 1033 arXiv:0907.4290.

1034

1035 Sornette D, Ouillon G (2012) Dragon-kings: mechanisms, statistical methods and empirical
 1036 evidence. *The European Physical Journal Special Topics*, 205(1), 1-26.

1037

1038 Tabor M (1989) *Chaos and Integrability in Nonlinear Dynamics*; Wiley: New York, NY, USA, 1989

1039

1040 Tormann T, Wiemer S, Mignan, A (2014) Systematic survey of high-resolution b value imaging along
 1041 Californian faults: Inference on asperities. *Journal of Geophysical Research: Solid Earth*, 119(3),
 1042 2029-2054. <https://doi.org/10.1002/2013JB010867>

1043

1044 van der Elst NJ (2021) B-positive: A robust estimator of aftershock magnitude distribution in
 1045 transiently incomplete catalogs. *Journal of Geophysical Research: Solid Earth*, 126(2),
 1046 e2020JB021027

1047

1048 Vassiliou MS, Kanamori H (1982) The energy release in earthquakes. *Bulletin of the Seismological
 1049 Society of America* 72(2): 371–387. <https://doi.org/10.1785/BSSA0720020371>

1050

1051 Venegas-Aravena P, Cordaro E, Laroze D (2022) Fractal Clustering as Spatial Variability of Magnetic
1052 Anomalies Measurements for Impending Earthquakes and the Thermodynamic Fractal Dimension.
1053 *Fractal and Fractional* 6(11):1-13. <https://doi.org/10.3390/fractalfract6110624>
1054

1055 Venegas-Aravena P (2023) Geological earthquake simulations generated by kinematic
1056 heterogeneous energy-based method: Self-arrested ruptures and asperity criterion. *Open*
1057 *Geosciences* 15(1):1-20. <https://doi.org/10.1515/geo-2022-0522>
1058

1059 Venegas-Aravena P, Cordaro E (2023a) Subduction as a Smoothing Machine: How Multiscale
1060 Dissipation Relates Precursor Signals to Fault Geometry. *Geosciences* 13(8):1-16.
1061 <https://doi.org/10.3390/geosciences13080243>
1062

1063 Venegas-Aravena P, Cordaro E (2023b) Analytical Relation between b-Value and Electromagnetic
1064 Signals in Pre-Macroscopic Failure of Rocks: Insights into the Microdynamics' Physics Prior to
1065 Earthquakes. *Geosciences* 13(6), 169:1-14. <https://doi.org/10.3390/geosciences13060169>
1066

1067 Venegas-Aravena P (2024a) Heterogeneous self-arrested ruptures leading to spatial variability of
1068 radiated energy and Doppler effect of the observed corner frequency. *Journal of Seismology* 28(1):
1069 187–208. <https://doi.org/10.1007/s10950-023-10183-3>
1070

1071 Venegas-Aravena P (2024b) Past large earthquakes influence future strong ground motion:
1072 Example of the Chilean subduction zone. *Natural Hazards* 120(1): 10669–10685.
1073 <https://doi.org/10.1007/s11069-024-06651-9>
1074

1075 Venegas-Aravena P, Cordaro E (2024) The Multiscale Principle in Nature (*Principium luxuriæ*):
1076 Linking Multiscale Thermodynamics to Living and Non-Living Complex Systems. *Fractal and*
1077 *Fractional* 8(1):1-43. <https://doi.org/10.3390/fractalfract8010035>
1078

1079 Venegas-Aravena P, Crempien JGF, Archuleta RJ (2024) Fractal Spatial Distributions of Initial Shear
1080 Stress and Frictional Properties on Faults and Their Impact on Dynamic Earthquake Rupture.
1081 *Bulletin of the Seismological Society of America* 114(3): 1444–1465.
1082 <https://doi.org/10.1785/0120230123>
1083

1084 Vidale JE, Agnew DC, Johnston MJ, Oppenheimer DH (1998) Absence of earthquake correlation
1085 with Earth tides: An indication of high preseismic fault stress rate. *Journal of Geophysical Research:*
1086 *Solid Earth*, 103(B10), 24567-24572. <https://doi.org/10.1029/98JB00594>
1087

1088 Vieira MdS (1999) Chaos and Synchronized Chaos in an Earthquake Model. *Physical Review Letters*
1089 82(1): 201-204. <https://doi.org/10.1103/PhysRevLett.82.201>
1090

1091 Wallace LM, Fagereng Å, Ellis S (2012) Upper plate tectonic stress state may influence interseismic
1092 coupling on subduction megathrusts. *Geology* 40(10): 895–898. <https://doi.org/10.1130/G33373.1>
1093

1094 Wang Z, Zhang W, Taymaz T, He Z, Xu T, Zhang Z (2023) Dynamic Rupture Process of the 2023 Mw
1095 7.8 Kahramanmaraş Earthquake (SE Türkiye): Variable Rupture Speed and Implications for Seismic
1096 Hazard. *Geophysical Research Letters* 50(15):1-11. <https://doi.org/10.1029/2023GL104787>
1097

1098 Wetzler N, Lay L, Brodsky EE (2023) Global Characteristics of Observable Foreshocks for Large
1099 Earthquakes. *Seismological Research Letters* 94(5): 2313–2325.
1100 <https://doi.org/10.1785/0220220397>
1101

1102 Wiemer S, Wyss M (1997) Mapping the frequency-magnitude distribution in asperities: An
1103 improved technique to calculate recurrence times?. *Journal of Geophysical Research: Solid Earth*,
1104 102(B7), 15115-15128. <https://doi.org/10.1029/97JB00726>.
1105

1106 Woessner J, Wiemer S (2005) Assessing the quality of earthquake catalogues: Estimating the
1107 magnitude of completeness and its uncertainty. *Bulletin of the Seismological Society of America*,
1108 95(2), 684-698. <https://doi.org/10.1785/0120040007>
1109

1110 Wu G-C, Baleanu D (2015) Jacobian matrix algorithm for Lyapunov exponents of the discrete
1111 fractional maps. *Communications in Nonlinear Science and Numerical Simulation* 22(1–3): 95-100.
1112 <https://doi.org/10.1016/j.cnsns.2014.06.042>
1113

1114 Wyss M (1997) Cannot Earthquakes Be Predicted? *Science* 278(5337): 487-490.
1115 <https://doi.org/10.1126/science.278.5337.487>
1116

1117 Wyss M, Sammis CG, Nadeau RM, Wiemer S (2004) Fractal Dimension and b- Value on Creeping
1118 and Locked Patches of the San Andreas Fault near Parkfield, California. *Bulletin of the*
1119 *Seismological Society of America* 94 (2): 410–421. <https://doi.org/10.1785/0120030054>
1120

1121 Xie H (1993) *Fractals in Rock Mechanics*, 1st ed.; CRC Press: Boca Raton, FL, USA
1122

1123 Yılmaz N, Akıllı M, Ak M (2023) Temporal evolution of entropy and chaos in low amplitude seismic
1124 wave prior to an earthquake. *Chaos, Solitons & Fractals* 173(1): 1-11.
1125 <https://doi.org/10.1016/j.chaos.2023.113585>
1126

1127 Zaccagnino D, Doglioni C (2022) The impact of faulting complexity and type on earthquake rupture
1128 dynamics. *Communications Earth & Environment*, 3(1), 258. [https://doi.org/10.1038/s43247-022-](https://doi.org/10.1038/s43247-022-00593-5)
1129 [00593-5](https://doi.org/10.1038/s43247-022-00593-5).
1130

1131 Zaccagnino D, Vallianatos F, Michas G, Telesca L, Doglioni C (2024) Are Foreshocks Fore-Shocks?
1132 *Journal of Geophysical Research* 129(2): 1-17. <https://doi.org/10.1029/2023JB027337>
1133

1134 Zou X, Fialko Y (2024) Can Large Strains Be Accommodated by Small Faults: “Brittle Flow of Rocks”
1135 Revised. *Earth and Planet Science* 11(11): 1-16. <https://doi.org/10.1029/2024EA003824>